ACS MATERIALS LETTERS

www.acsmaterialsletters.org

Sequential Activation of Spatially Localized Oligonucleotides

Moshe Rubanov, Phillip J. Dorsey, Dominic Scalise, and Rebecca Schulman*

Cite This: *ACS Materials Lett.* 2022, 4, 1807−1814

Read Online

ACCESS | Metrics & More | Article Recommendations | Supporting Information

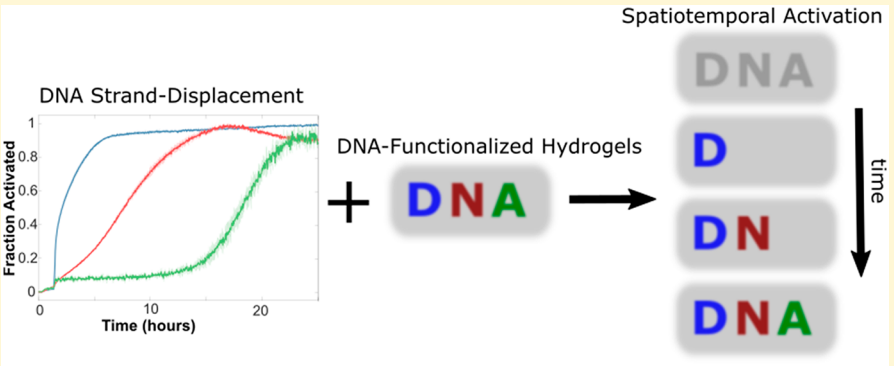

ABSTRACT: **The programmable spatiotemporal activation of molecules could be used to create stimuli-responsive biomaterials capable of executing multistage sensing and computational processes. Here we develop a method for the activation of different DNA molecules in precisely specified locations and times within hydrogels. The activation locations are determined by patterning molecules to be released in their inactive form within hydrogels at resolutions of tens of microns, whereas the time of activation is controlled by a DNA strand displacement reaction cascade that releases the target DNA oligonucleotides at precisely specified time intervals. This programmed activation of DNA from hydrogel substrates thus enables the scalable development of DNA-based reaction-diffusion systems that regulate DNA strand availability in space and time. This system could be used as a platform to autonomously activate predefined chemical signals embedded within a soft material.**

Cells and tissues execute a multitude of spatially and temporally controlled chemical processes giving rise to the structural organization of organisms. In the context of developmental biology, the shape, size, and duration of morphogen gradients hold critical functions for inducing disparate pathways of tissue differentiation during embryogenesis. For example, during vertebrate dorsal-ventral patterning, progenitor domains that eventually constitute ventral body segments form in a sequential and directional manner in response to morphogen gradients of signaling proteins.[1] Specifically, spatial information, encoded as such gradients, induces a *programmed order and time scale* of pattern presentation and development across tissues in a concentration-dependent manner via genetic regulatory feedback.

Synthetic reaction-diffusion systems that mimic spatiotemporal regulatory mechanisms in biological systems have been developed to program complex behaviors in synthetic materials. Recently, *in vitro* genetic circuits that respond to chemical gradients via artificial emulsion-based cellular compartments have been used to direct the propagation of signals, allowing for the controlled differentiation of artificial cells, suggesting how spatial and temporal control of chemical activity can induce the formation of geometrically defined chemical patterns.[2] Additionally, spatiotemporal signal control in synthetic sender-receiver systems has been used for distributed information processing, which can achieve processes such as distributed memory storage.[3] Joesaar et al. implemented a specific application of distributed information processing in a synthetic reaction-diffusion system using a microfluidic array of sender-receiver "protocells" that communicated with nearby cells and interpreted incoming communication signals with DNA computations.[4]

A variety of platforms have also been developed for executing robust, controlled, spatiotemporal activation of chemical species

Received: April 1, 2022
Accepted: August 12, 2022

within hydrogel substrates through mechanisms that release and/or modify the chemical species embedded within the material.[5−10] Hydrogels have been studied extensively due to their potential for recapitulating biological environments, such as 3D cell cultures.[11] Deforest and Tirrell anchored a variety of proteins in hydrogels in three-dimensional space using light-initiated click chemistry and subsequently released portions of the anchored protein by further exposure to light.[5] Azagarsamy and Anseth demonstrated the selective cleavage of proteins and other target molecules using orthogonal wavelengths, thereby attaining spatial control of activation within the matrix.[6] Importantly, independent activation of molecules within these hydrogels have been shown with externally applied stimuli such as spatially modulated light exposure, after initialization, limiting autonomous material response.

Programming cell-responsive matrices is another route toward achieving self-directed chemical activation in synthetic biomaterials; having a portion of the matrix that can be degraded by extracellular proteases enables responsivity tailored to cell proliferation and migration.[7] Studies have also examined how either spatial *or* sequential activation of target molecules might be achieved using physical and kinetic mechanisms. These include the triggered release of target molecules (such as signaling proteins), using intertwined degradable and non-degradable polymeric matrices,[8] changing molecular weights of degradable matrices for controlled release of gene-editing lentiviral vectors,[9] leveraging 3D-printed coaxially electrospun polymers with tunable rates of diffusion,[10] and a DNA-based sequential release avalanche for controlled release of nanoparticles from hydrogels.[12] This last example uses both strand-displacement (a chemical process) and nanoparticle separation by the material to achieve sequential release.

Each of these strategies rely on the physical properties of the material itself to control how activation occurs. Here we investigate whether multistep activation processes might occur in specific spatial regions of a material by encoding sets of instructions as a chemical program. Specifically, we show how a programmable chemical reaction network can regulate the times and locations of sequential activation within a material.

The resulting approach allows for autonomous activation of unique target molecules at different, predetermined times and locations within a hydrogel without changing the structure of the hydrogel matrix. We use DNA oligonucleotides to sequentially release unique orthogonal products. Based on the combinatorial sequence phase space provided by Watson−Crick base-pairing and the binding specificity of DNA hybridization, many sequential activation stages could be achieved. Additionally, each orthogonal DNA strand programmed for activation from the hydrogel could be modified with other small molecules or proteins to modulate other hydrogel activation applications.[13−15] The DNA-based reaction cascade is designed so that the amount of reactant released, and time scales of activation, can be quantitatively varied using clear design rules.

To attach our DNA complexes to a polymeric matrix, we build on work by Dorsey et al.[16] who used a photopolymerization reaction to link DNA strands to a polyethylene glycol diacrylate (PEGDA) hydrogel. To program specific spatial DNA strand activation, we cross-link unique modified DNA strands in localized hydrogel domains using digital photolithography[16] (Figure 1). Lastly, to regulate the timing of DNA strand activation from different locations, we implement a DNA-based chemical reaction network that sequentially releases strands that can trigger actuation of the spatially anchored target strands.[13]

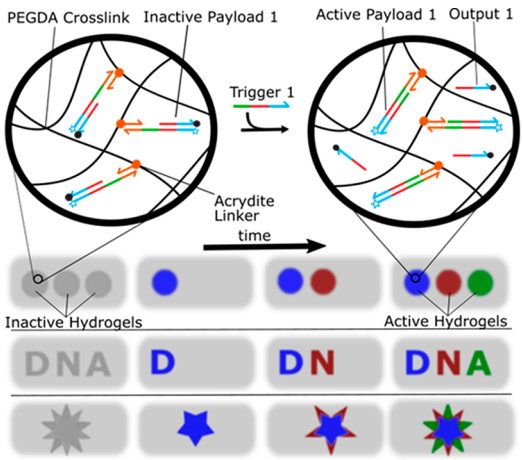

Figure 1. DNA complexes (inactive Payloads) are localized within specific regions of (PEGDA) hydrogels via Acrydite linkers. Release of quencher-labeled strand in the inactive Payload (the Output) via a reaction with Trigger 1 activates the Payload.

We developed a platform for autonomously controlling three or more chemical activation processes in a substrate at different locations and over multiple time steps, each spanning the order of a few hours. Such autonomous control of molecular activation within a soft material could be used in applications such as drug delivery,[17,18] and the development of smart micromaterials with the capability to sense and/or heal,[19−21] and undergo chemical locomotion[22−25] or chemomechanical actuation.[26,27]

Here we studied the spatiotemporal control of the activation (i.e., chemical/conformational change) of DNA complexes conjugated to a hydrogel (Figure 1). Activation is the strand-displacement reaction of a double stranded (ds) DNA complex that changes its conformation. This reaction is a toehold-mediated strand displacement reaction, i.e., a reaction in which a DNA strand binds to an exposed toehold, or single-stranded region on a DNA complex, displacing one or more of the strands in the complex. This process also displaces a DNA strand with a quencher label so that activation leads the complex to fluoresce and releases an output strand that can then freely diffuse. The sequences of the complex and the released strand can be chosen by design, and in principle, the chemical labels or sequences on an output strand could be swapped so that other changes in chemical functionality could be achieved through activation. For example, the sequence of the strand that is released could be conjugated to proteins, mRNA, or small molecules[28−31] to direct these species release in tandem.

We previously demonstrated that strand displacement cascades could regulate the times at which different oligonucleotide complexes were activated in well-mixed solution,[13] i.e., that activation can be temporally controlled. We ask how this method might be used to exert spatiotemporal control over activation. To do so, we first chose a prototype temporal control circuit that activates three different oligonucleotide complexes in a specific, timed sequence. This activation is orchestrated by a reaction cascade that directs reaction stages that proceed one after another. During each stage, a pair of reactions can occur: a Conversion reaction and a Payload Activation reaction (Figure 2). A Payload Activation reaction releases a single strand with a specific sequence. The cascade was designed so that the timing of activation and the amount of each complex released during each stage can be adjusted by changing the concentrations of the reactants.

https://doi.org/10.1021/acsmaterialslett.2c00286
ACS Materials Lett. 2022, 4, 1807−1814

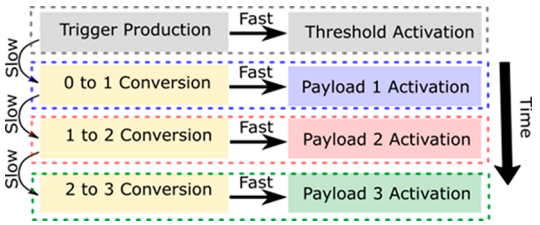

Figure 2. Overview of a chemical reaction network that orchestrates sequential Payload Activation. Reactions are shown as solid shaded rectangles. A slow reaction in the Trigger Activation reaction releases a species $Trigger_0$ that first reacts with a Threshold complex until it is depleted, creating a delay before the start of the release of $Trigger_1$ via a much slower reaction. Stages, indicated by dashed rectangles surrounding pairs of reactions, then execute a series of paired fast depletion reactions, direct activation through reactions with a Payload and Conversion reactions that produce $Trigger_{i+1}$ in a reaction between $Trigger_i$ and a corresponding Convert complex (see Figure 3a–c). Stage 0: gray dashed rectangle, Stage 1: Blue dashed rectangle, Stage 2: Red dashed rectangle, Stage 3: Green dashed rectangle.

The sequential activation process is orchestrated by a Trigger Production reaction which initiates the downstream stages (Figure 3a). The Trigger production reaction occurs between a single-stranded Initiator and double-stranded Source complex that are supplied in significant excess of all other reactants so that the reaction continues through the entire activation process. The reaction between Source and Initiator thus provides the driving force that propels the entire reaction cascade (SI Sections S1 and S2). The Initiator and Source react via a strand-displacement reaction mediated by a 0-nucleotide (nt) length toehold and therefore proceed slowly (approximately $5 \times 10^{-7} \mu M^{-1}\ s^{-1}$)[32] to continuously produce $Trigger_0$, a ssDNA species.

The prototype activation reaction network contains three stages in which Payloads are activated. Before these three stages begin, Threshold Activation occurs during what we term Stage 0 (Figure 2). During Threshold Activation, $Trigger_0$ reacts with a Threshold species in a 7 nucleotide (nt) toehold-mediated strand displacement reaction (Figure 3b). This Thresholding reaction acts to delay the start of the subsequent stages (SI Sections S3 and S4). The 0 to 1 Conversion reaction, which is the start of Stage 1, is mediated by a 4-nt toehold, while the Payload 1 activation reaction is a 7-nt toehold-mediated reaction. The rate constant for the 4-nt toehold mediated Conversion reaction is therefore 3 orders of magnitude smaller than the rate constant for a 7-nt toehold mediated Payload Activation reaction, which means that the Conversion reaction begins to occur once the Threshold species is depleted[32] (Figure 3c). Each of the three subsequent stages consist of a Conversion reaction and a Payload Activation reaction. Progress through the stages is driven by the continual infusion of $Trigger_0$ from the Trigger Production reaction.

Stage 1, like Stage 0, involves two reactions that have very different rates. The first reaction, 0–1 Conversion, releases that stage's Trigger ($Trigger_1$) when $Trigger_0$ reacts with $Convert_{0-1}$, a double-stranded species, via a 4-nt toehold reaction (Figure 3b). The second reaction, Payload 1 Activation, then sequesters the released trigger to activate the Payload: $Trigger_1$ reacts via a 7-nt toehold reaction with a fluorescently labeled $Payload_1$ complex to displace $Output_1$, a quencher strand. Stages 2 and 3 have the same structure as Stage 1. In Stage 2, $Trigger_1$ reacts with $Convert_{1-2}$ in a 4-nt initiated toehold reaction to release $Trigger_2$; $Trigger_2$ then reacts with $Payload_2$ via a 7-nt toehold to

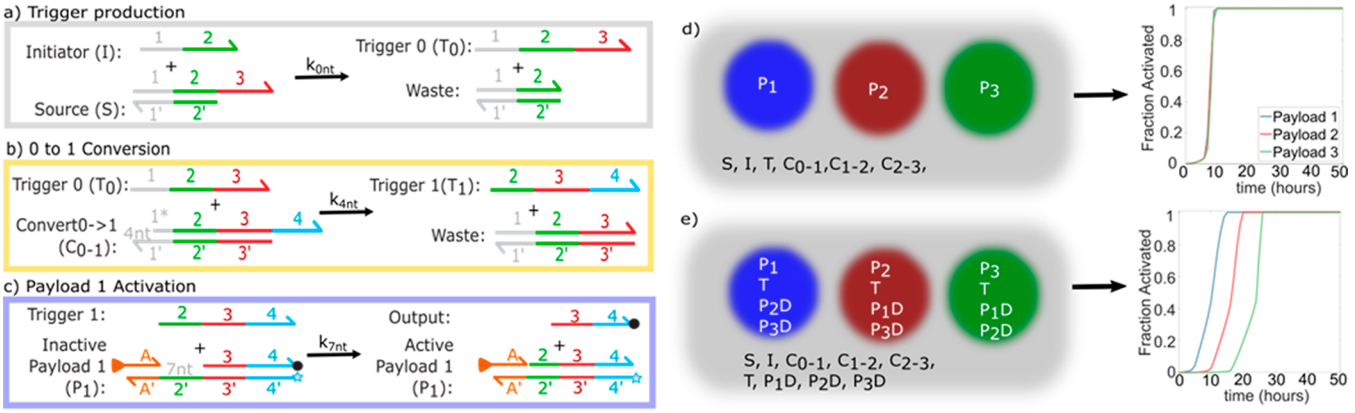

Figure 3. Example reactions from the sequential activation reaction cascade and reaction-diffusion simulations. DNA domains each have unique labels (number or letter). Complementary domains have the same labels with and without an apostrophe (e.g., domain 1 is complementary to domain 1′). Sequences are given in Table S1 and Figure S1. (a) The Initiator and Source react to produce Trigger 0. Because there is no toehold to initiate the reaction, the reaction's rate constant is very low (approximately $k_{0nt} = 2 \times 10^{-6} \mu M^{-1}\ s^{-1}$).[32] (b) Each Trigger i (i = 0 shown here as an example) reacts with its respective Convert complex (here 0–1) to produce Trigger i+1 in a 4-nucleotide toehold-initiated strand displacement reaction. The reaction effectively thereby converts Trigger i into Trigger i+1 via a reaction with a small rate constant ($k_{4nt} = 2 \times 10^{-2} \mu M^{-1}\ s^{-1}$).[32] (c) Each Trigger i (1 shown here as an example) reacts with its respective inactivated Payload to activate the Payload and release an Output in a 7-nucleotide toehold strand-displacement reaction ($k_{7nt} = 4 \mu M^{-1}\ s^{-1}$).[32] Payload activation removes a quencher from the Payload complex, leaving a fluorescent, i.e., active, Activated Payload. (d,e) Reaction-diffusion simulations of Payload activation beginning from initial conditions (left) in which the stated species are present either in solution (gray) or conjugated to a hydrogel (red, green, or blue). Species shown in white text are those initially conjugated to the hydrogel polymer network while species shown in black text are those initially present in solution. (d) Payloads are localized within the hydrogel and Source, Initiator, Threshold, and Convert complexes (S,I, T and Cn-n+1) are in solution. Because there are no Payloads in solution, the reaction progresses without the desired delays -- the Payloads are instead all activated in rapid succession. (e) In a process in which damper (nonfluorescent) Payloads (P1D, P2D, P3D) are both in solution and in the hydrogels, Payloads are activated in the hydrogel at distinct times with approximately 10 h of separation. (d,e) Hydrogel depictions are not to scale. (d,e) In the model, the hydrogels had 150 μm radii with 100 μm spacing between hydrogels (edge to edge).

https://doi.org/10.1021/acsmaterialslett.2c00286
ACS Materials Lett. 2022, 4, 1807–1814

activate $Output_2$, generating fluorescence. In Stage 3, likewise, $Trigger_2$ reacts with $Convert_{2-3}$ in a 4-nt initiated toehold reaction to activate $Trigger_3$ and $Trigger_3$ reacts with $Payload_3$ to release $Output_3$, producing a fluorescence signal that can be used to track reaction progress. Additional activation steps could be added to this cascade by adding new stages consisting of paired Conversion and Payload Activation reactions.

Because of the difference in reaction rate constants of the Conversion and Payload Activation reactions, only after $Payload_n$ is completely reacted can $Trigger_n$ react with $Convert_{(n)-(n+1)}$ species to release $Trigger_{n+1}$ for the next stage (Figure 3a−c). These reactions therefore enforce the order at which the reactions occur in the cascade. The circuit is designed so that rate of progression through the different stages of sequential activation is controlled by the rate of Trigger production, i.e., the rate of reaction between Initiator and Source. The reaction cascade is designed so that each Payload is completely activated during its respective stage. Therefore, the concentration of the Payload activated is controlled by the initial concentration of the inactive Payload. One Output strand is released during activation, so the concentration of Output strand released is also equal to the initial concentration of inactive Payload that is sequestered in the hydrogel (Figure 3c). Correspondingly, the circuit is designed so that the delay between the end of one activation stage and the beginning of the next should be proportional to the concentration of the Convert complex. If concentrations of the Payloads, Convert complexes, Initiator, and Source can be varied from nanomolar to micromolar, sequential activation cascades using the same toehold lengths could be designed that would activate micromolar to nanomolar concentrations of Payloads in each stage over minutes to hours, with stages of activation being separated from 1 to 10 h.

We hypothesized that such a circuit could also control where and when different Payloads were activated within a hydrogel with approximately the same control over activation times that was achieved in a well-mixed solution if certain reactants were each localized to different hydrogel regions. To evaluate this hypothesis, we considered whether we could control both when and where a set of Payloads were activated in the example activation cascade in Figures 2 and 3a−c. To construct this cascade, we chose example Source, Initiator, Convert, Threshold, and Payload sequences (SI Table S2) and concentrations of each of these complexes that would lead to 100 nM of Payload being activated approximately every 10 h at each stage. At these reactant concentrations, the rate constants of the strand displacement reactions imply that the fast activation process at the beginning of each stage should be completed in less than 1 h, while the slow conversion following each stage of activation should take 5−10 h (SI Section S2).[32] As a result, each activation process should happen 5−10 h after the last. We tested the times that each Payload reached 50% activation in an experiment using time-domain fluorescence measurements. We found that 50% of the three Payloads were activated at 2, 8, 18 h, respectively (Figure S2b), consistent with this prediction.

We next asked how we might activate each of the different Payloads in unique hydrogel regions according to the activation schedule of the sequential activation circuit. We initially hypothesized that we would be able to recapitulate the activation schedule that the cascade directed in well-mixed solution, while localizing activation, by anchoring each of the Payloads anchored within unique hydrogels to control where activation occurred, and by adding the remaining reactants to the surrounding solution.

We tested this hypothesis by asking what the activation schedule would be within an example environment consisting of three hydrogel cylinders of radius 150 μm, with 100 μm spacing between the circles' edges. In this environment, 100 nM of one of the three types of Payload species was anchored within each of the three circular hydrogel domains (Figure 3 and SI Figure S3); the areas surrounding the hydrogels was aqueous buffer containing Threshold Payload, $Convert_{0-1}$, $Convert_{1-2}$, and $Convert_{2-3}$ (SI Section S2).

To predict the activation schedule, we developed simulations of the reaction-diffusion process that would unfold in such an environment. We then sought to measure the predicted times at which each of the three locally sequestered Payloads reached 50% activation. These simulations used coupled PDEs that were derived from coupled ODEs that model the reactions the sequential activation cascade (SI Section S5). We assumed that the diffusion constants for ssDNA and DNA complexes were both ($D_{ss} = D_{ds} = 60\ \mu m^2/s$) inside the hydrogels.[16] We also assumed that the biomolecular rate constants between the DNA species were the reported average rate constants for strand-displacement reactions with the corresponding toehold lengths in solution.[13,32−34] In the aqueous buffer, the DNA diffusion coefficients were also assumed to be the same for ssDNA and DNA complexes and were set at $D_{ss} = D_{ds} = 150\ \mu m^2/s$.[13] The initial concentrations of the Initiator and Source species were each 2 μM in the solution outside the hydrogel and 0 μM within the hydrogel. The concentrations of each of the initial Convert complex were 0 nM inside the hydrogel. In the solution outside the hydrogel, the initial concentrations were set to $Convert_{1-2}$ = 450 nM, $Convert_{2-3}$ = 300 nM, $Convert_{3-4}$ = 150 nM (Figure 3d, SI section S5 and Table S1). The initial concentration of each Payload species was 100 nM within its respective cylindrical hydrogel and 0 nM elsewhere. The simulations were run in COMSOL 5.1 using a two-dimensional geometry consisting of three circles with the radii of the cylinders we designed at the prescribed separation.

The schedule of activation observed in these simulations was not the expected schedule in which the times at which each of the stages reached 50% were separated by 10 h. Instead, during the simulation, all Payloads were activated at roughly the same time, rather than the Payloads being activated in sequential stages separated by 10 h as they were in well-mixed solution (Figure 1d).

To understand this behavior, we looked at the concentrations of the different species across the reaction environment and over time and compared these concentrations to those predicted by the simulation of the same sequential activation process in well-mixed solution. We found that Trigger 1, 2, and 3 molecules were released much faster in the spatiotemporal activation process we designed than in the well-mixed solution. We hypothesized that these differences in timing were caused by the fact that in the spatiotemporal activation process, the Payloads were present only within the hydrogels and not in the surrounding solution. A Payload for a given stage acts as a sink for that stage's Trigger molecule, and only after all the Payload is activated should that trigger molecule react with the Convert species that releases the Trigger for the next stage. Over time in the simulation, $Trigger_n$ accumulates faster in the solution than in the hydrogels, but in solution, there is no Payload to react with it. Even though the Payload in the hydrogels is not yet depleted, $Trigger_n$ can react with its

https://doi.org/10.1021/acsmaterialslett.2c00286
ACS Materials Lett. 2022, 4, 1807−1814

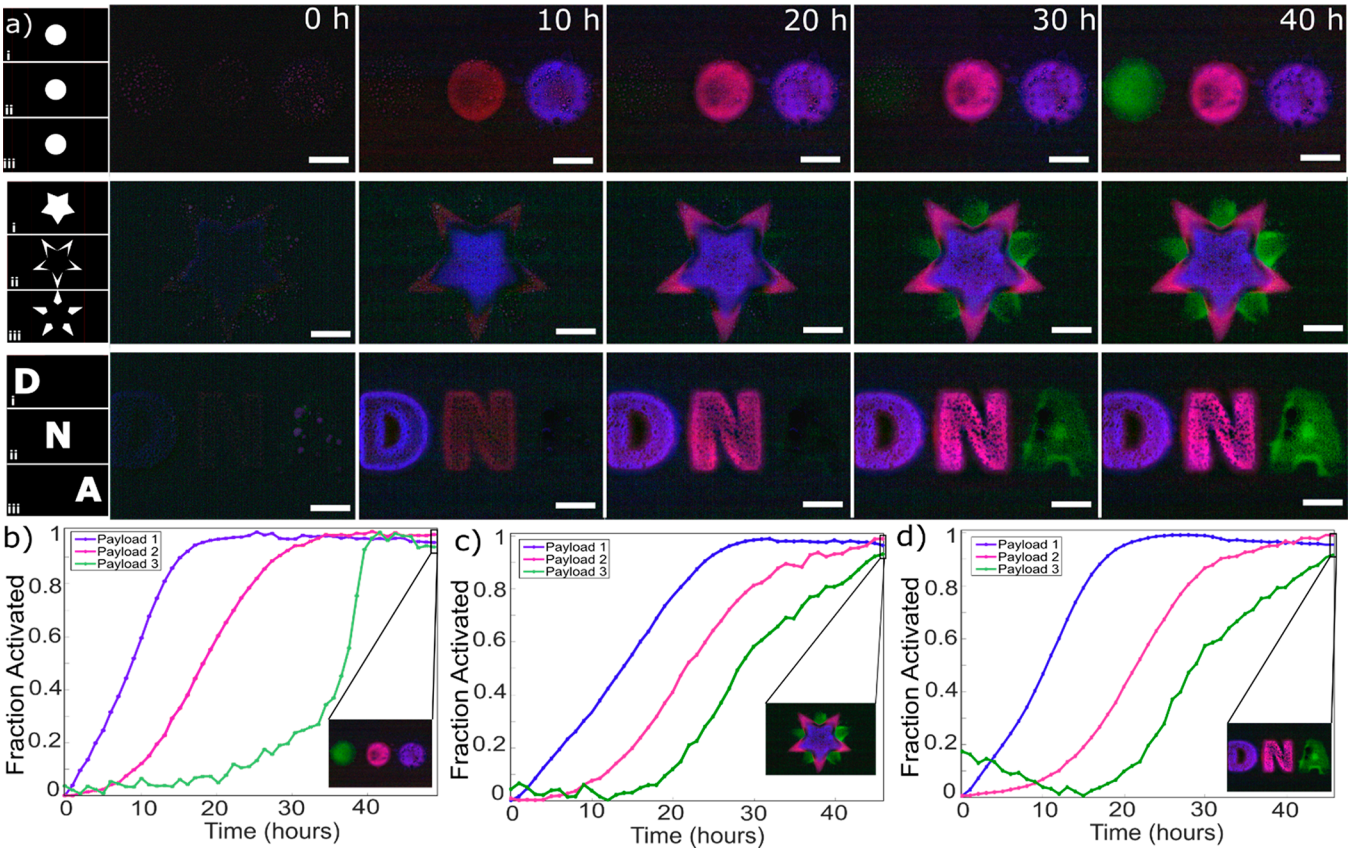

Figure 4. Sequential activation of Payloads within multidomain hydrogels. (a) Three different gel domains activated sequentially over a span of 50 h using the DNA strand-displacement circuit shown in Figure 2 (sequences and concentrations in SI Table S1 and S2). The hydrogels and the Payloads and Convert complexes are initialized as shown in Figure 3e. Binary masks used to photopolymerize each domain are shown as subpanels to the left of the *t* = 0-h micrographs. (b−d) Spatially averaged fractions of activation of the three patterned domains over time. (b) Fraction of activation of three patterned cylindrical hydrogels shown in the top panel of (a). (c,d) Fraction activated of the hydrogels shown in the middle and bottom panels of a, respectively. Panels b−d are generated as described in Section S9.

corresponding Convert complex, allowing the next stage to begin. The cumulative effect of the premature initiation of new stages outside of the hydrogel domains is that multiple stages can proceed in tandem, so that $Payload_{n+1}$ begins to activate before $Payload_n$ activation completes. For example, within the hydrogel containing $Payload_2$, $Trigger_2$ will tend to first react with an anchored $Payload_2$ prior to reacting with a $Convert_{2-3}$ species because both are present within the gel and the reaction with $Payload_2$ is much faster than the reaction with $Convert_{2-3}$. However, in the surrounding solution, $Convert_{2-3}$ is present, but $Payload_2$ is not. Thus, $Trigger_2$ reacts with $Convert_{2-3}$ before the $Payload_2$ in the hydrogel is depleted.

Payloads thus act as a damper for downstream Trigger release occurring through conversion reactions. Because the solution outside of the hydrogels contains no Payload, Trigger is released in this solution more rapidly than it is within the hydrogel regions that contain the Payload for that Trigger species. We therefore hypothesized that proper delays in activation could be restored by introducing molecules that act as dampers for Trigger accumulation outside of the hydrogels where activation should occur. We designed damper Payloads ($Payload_{Dn}$) that react with their respective Trigger species at the same rate as regular Payloads but during this reaction, the damper Payloads do not become fluorescent, and thereby are "nonfunctional" (SI Figure S4). In other cases, the output strand of a Payload could be conjugated to mRNA, aptamer, protein, or other small molecules, so that the output of a damper Payload could be nonfunctional in that it lacked these modifications. Simulations of the spatiotemporal activation process in which 100 nM of each $Payload_D$ was presented initially solution, produced the desired kinetics of activation for the hydrogel: an initial delay of roughly 5 h for 50% activation of the first hydrogel patterned with $Payload_1$ followed by roughly 10 h of separation between the activation of each subsequent Payload patterned within the respective hydrogel domains (Figure 3e).

Simulations also suggested a key advantage of this design: the timing of a given Payload's activation program was not significantly affected by the size or shape of the region it should be activated from (SI Figure S5). This observation suggests that the method for designing sequential activation process and adopting them for spatiotemporal control using patterning and damper payloads could be a general approach for designing spatiotemporal activation schedules for a wide variety of patterned hydrogel structures. Simulations also showed that when the concentration of Payload was decreased and $Payload_D$ increased so that the sum of the concentrations of $Payload_D$ and Payload was unchanged, the concentration of Payload activated was altered but the timing of activation cascade was unaffected (SI Figure S6).

Varying the diffusion constants of all the ssDNA and DNA duplexes in solution and in hydrogel over 2 orders of magnitude in our simulations resulted in almost no change in activation rates or activation timing (SI Figure S7), suggesting that the sequential activation cascade could direct spatiotemporal release

https://doi.org/10.1021/acsmaterialslett.2c00286
ACS Materials Lett. 2022, 4, 1807−1814

of molecules of different sizes within a range of hydrogels with different mesh sizes. Varying all the rate constants for the reactions of the sequential activation cascade, in contrast, had a strong influence on the activation schedule: lowering each of the rate constants of the 0-nt 4-nt, and 7-nt toehold strand displacement reactions by 50% caused the times at which 50% activation for each stage occurred to double (SI Figure S8). Therefore, the hydrogel sequential activation process we designed is expected to operate in a reaction-limited rather than diffusion-limited regime.

Simulations also indicated that all the Payload complex sequestered in the gel is activated at that location (SI Figure S9). This result suggested that when patterning the hydrogels that contain Payloads, controlling the concentration of Payload that gets activated requires controlling how much DNA is patterned in each hydrogel domain.

To make hydrogel domains where the amount of DNA patterned within them is well-controlled, we used digital photopatterning to generate DNA-functionalized PEGDA hydrogels (PEGDA (Mn = 575), a UV photoinitiator (Omnirad 2100)) within microfluidic flow cells[16] (see SI Section S6 and Figure S10 for process details). To determine the concentration of DNA in patterned hydrogels, we measured how much DNA remained photopolymerized to the hydrogel, i.e., the cross-linking efficiency of DNA. We photopolymerized hydrogels containing a dsDNA complex, (Payload 3 without the hybridized quencher strand, termed P3FA) consisting of a strand with an acrydite group hybridized to a strand with a fluorophore modification, so that changes in fluorescence could be used to quantify cross-linking efficiency (see SI Table 2 for sequences). The dsDNA complex was photopatterned within a cylindrical hydrogel with radius 150 μm and height 100 μm were polymerized containing 100 nM P3FA. To remove non-cross-linked DNA, we then washed the gel with aqueous buffer for 12 h using the washing protocol detailed in Dorsey et al.[16] The change in fluorescence of the hydrogel when comparing the gel directly after photopatterning to the same gel after the 12-h wash indicated a cross-linking efficiency of DNA of 55 ± 3.9% (n = 3 gels, mean ± s.d.). This cross-linking efficiency is consistent with similar photopatterning processes[35−37] (SI Section S7 and Figure S11). We thus assumed half of the Payloads would remain conjugated to the hydrogel after photopolymerization in subsequent experiments.

To test the spatiotemporal activation process we designed, we patterned three separate 150 μm diameter cylinders such that the first cylinder contained anchored $Payload_1$, Threshold, and $Payloads_{D2,3}$, the second hydrogel contained anchored $Payload_2$, Threshold, and $Payloads_{D1,3}$, and the third hydrogel contained anchored $Payload_3$, Threshold, and $Payloads_{D1,2}$. After patterning each of the cylinders and washing them to remove unanchored DNA, we next added solution to the microfluidic flow cell containing the Source, Initiator, and the Convert, Threshold, and freely diffusing $Payloads_D$ species for each of the three stages. The concentrations of each molecule inside each hydrogel and the surrounding solution were those designed and tested in the simulation and are given in Figure 3e and SI Table S1. We hypothesized that the cascade would activate the stages sequentially according to the programmed schedule of activation (Figure 4a). We observed that after the reactant solution was added, the Payloads in the three cylindrical domains activated sequentially. The three hydrogels reached 50% activation after 10, 19, and 36 h, respectively (Figure 4b), consistent with the predictions of the simulations.

We next asked whether the times at which the different Payloads activated were largely independent of the sizes and shapes of hydrogel domains containing the Payloads, as the simulations predicted (SI Figure S5). To do so, we created two additional three-domain hydrogel patterns (Figure 4a) in which the same sets of Payloads and Threshold were anchored to each of the three domains as were in the experiments with three hydrogel cylinders. We added solution containing the same concentrations and types of DNA complexes (Source, Initiator, Convert, damper Payloads) surrounding each pattern as were used in the experiments with three cylinders to sequentially activate the anchored Payloads in each hydrogel domain. The first cylinder (leftmost in Figure 1e) contained 100 nM of Payload 1, the second cylinder (center in Figure 1e) contained 100 nM of Payload 2, and the third cylinder (rightmost in Figure 1e) contained 100 nM of Payload 3. The leftmost hydrogel also contained 100 nM of Threshold, $Payload_{D2}$ and $Payload_{D3}$. Similarly, other two hydrogels contained 100 nM of Threshold and the two types of damper Payloads that were not present in their active forms. We observed similar activation times for both types of geometries: for the "D-N-A" pattern, mean 50% activation of stages 1, 2, and 3 corresponded to 11, 21, and 29 h (Figure 4a,c and Supplementary Video 1); for the concentric stars, the mean 50% stage activation corresponded to 14, 23, 28 h for stages 1, 2, and 3 respectively (Figure 4a,d and Supplementary Video 2). For all three hydrogel domains tested, we observed a mean separation between the activation of 50% of each stage of 9.7 ± 3.6 h (mean ± s.d.). These results support the hypothesis that diffusivity of the reaction species was not a significant factor for controlling stage activation behavior (SI Figure S7).

Here we demonstrate a means to autonomously direct activation of different DNA molecules at specific times and locations by leveraging photolithography to localize components and DNA-based chemical reaction networks to direct the timing of activation. We show that a molecular circuit which controls (1) the delay of activation of a payload and (2) the time over which a total dose of payload is activated, can likewise control the timing of these processes in a two-phase system consisting of hydrogel and surrounding solution. We further adopt this circuit to also control both where and when activation occurs in an architected hydrogel. Characterizing the dynamics of a model system of DNA-programmed pattern presentation within a hydrogel substrate facilitates the design of more sophisticated biomolecular programs of timed spatial pattern presentation. It might also be interesting to explore how to tune concentrations within the sequential activation circuit to induce specific activation schedules. Such systems could leverage transcriptional machinery to continuously and repeatably[38−41] execute designed spatiotemporal responses in conjunction with changing environmental cues or interface with small molecules or proteins using DNA/RNA aptaswitches.[15,42−44] One limitation to this system is that nucleases can degrade DNA, so that this circuit would not be expected to function in the manner observed here in environments where living cells produce these enzymes. Addressing this limitation, such as through circuit redesign, would be of interest for developing means to direct spatiotemporal release in 3D cell cultures or implanted substrates[11,45,46] or for use in tissue engineering applications.[47,48]

The material system developed here more generally enables autonomous control of the reaction network after initialization, which makes the system capable of undergoing a complex set of

https://doi.org/10.1021/acsmaterialslett.2c00286
ACS Materials Lett. 2022, 4, 1807−1814

spatiotemporal instructions to direct material composition or function without external intervention.

■ ASSOCIATED CONTENT

Supporting Information

The Supporting Information is available free of charge at https://pubs.acs.org/doi/10.1021/acsmaterialslett.2c00286.

Supporting video 1 (MP4)

Supporting video 2 (MP4)

Section S1, Sequential activation circuit design; Section S2, Selection of concentrations of sequential activation circuit components; Section S3, Purification protocol for reactant components; Section S4, Further purification of DNA complexes; Section S5, Reaction-diffusion model development; Section S6, Acrydite-modified DNA retention calculation; Section S7, Photopatterning of hydrogels and fabrication of microfluidic devices; Section S8, Data processing for fluorescence plots (PDF)

■ AUTHOR INFORMATION

Corresponding Author

Rebecca Schulman − *Department of Chemistry and Department of Computer Science, Johns Hopkins University, Baltimore, Maryland 21218, United States; Department of Chemical and Biomolecular Engineering, Johns Hopkins University, Baltimore, Maryland 21218, United States;* orcid.org/0000-0001-5129-5740; Email: rschulman@jhu.edu

Authors

Moshe Rubanov − *Department of Chemical and Biomolecular Engineering, Johns Hopkins University, Baltimore, Maryland 21218, United States;* orcid.org/0000-0001-8050-7407

Phillip J. Dorsey − *Department of Chemical and Biomolecular Engineering, Johns Hopkins University, Baltimore, Maryland 21218, United States;* orcid.org/0000-0002-0711-4428

Dominic Scalise − *Department of Chemical and Biomolecular Engineering, Johns Hopkins University, Baltimore, Maryland 21218, United States;* orcid.org/0000-0001-8218-1797

Complete contact information is available at: https://pubs.acs.org/10.1021/acsmaterialslett.2c00286

Author Contributions

M.R., R.S., and P.D. wrote the paper. D.S. and M.R. conceived of the idea. M.R. and P.D. designed the experiments, M.R. performed the experiments. All authors approved the final version of the manuscript.

Funding

This work was supported by DOE DE-SC0010426, with additional support from ARO W911NF2010057, DOE BES 221874, a JHU Catalyst Award and NSF SHF-1527377 to R.S. M.R. was supported by DOE DE-SC0010426 and ARO W911NF2010057, P.D. by the JHU Catalyst Award and DOE BES 221874, and D.S. by NSF SHF-1527377.

Notes

The authors declare no competing financial interest.

■ ACKNOWLEDGMENTS

The authors wish to thank Samuel Schaffter, Ruohong Shi, and Wenlu Wang for helpful advice and discussions.

■ ABBREVIATIONS

S, Source; I, Initiator; T, Threshold; C_{0-1}, Convert 0 to 1; C_{1-2}, Convert 1 to 2; C_{2-3}, Convert 2 to 3; P_1, Payload 1; P_2, Payload 2; P_3, Payload 3; P_{D1}, Damper Payload 1; P_{D2}, Damper Payload 2; P_{D3}, Damper Payload 3

■ REFERENCES

(1) Briscoe, J.; Small, S. Morphogen rules: design principles of gradient-mediated embryo patterning. *Development.* **2015**, *142*, 3996−4009.

(2) Dupin, A.; Simmel, F. C. Signalling and differentiation in emulsion-based multi-compartmentalized in vitro gene circuits. *Nature Chemistry.* **2019**, *11*, 32.

(3) Barcena Menendez, D.; Senthivel, V. R.; Isalan, M. Sender−receiver systems and applying information theory for quantitative synthetic biology. *Current Opinion in Biotechnology.* **2015**, *31*, 101−107.

(4) Joesaar, A.; Yang, S.; Bögels, B.; van der Linden, A.; Pieters, P.; Kumar, B.V.V.S.P.; Dalchau, N.; Phillips, A.; Mann, S.; de Greef, T. F. A. DNA-based communication in populations of synthetic protocells. *Nat. Nanotechnol.* **2019**, *14*, 369−378.

(5) DeForest, C. A.; Tirrell, D. A. A photoreversible protein-patterning approach for guiding stem cell fate in three-dimensional gels. *Nat. Mater.* **2015**, *14*, 523−531.

(6) Azagarsamy, M. A.; Anseth, K. S. Wavelength-Controlled Photocleavage for the Orthogonal and Sequential Release of Multiple Proteins. *Angewandte Chemie International Edition.* **2013**, *52*, 13803−13807.

(7) West, J. L.; Hubbell, J. A. Polymeric Biomaterials with Degradation Sites for Proteases Involved in Cell Migration. *Macromolecules.* **1999**, *32*, 241−244.

(8) Yonet-Tanyeri, N.; Rich, M. H.; Lee, M.; Lai, M.-H.; Jeong, J. H.; DeVolder, R. J.; Kong, H. The spatiotemporal control of erosion and molecular release from micropatterned poly(ethylene glycol)-based hydrogel. *Biomaterials.* **2013**, *34*, 8416−8423.

(9) Stilhano, R. S.; Madrigal, J. L.; Wong, K.; Williams, P. A.; Martin, P. K. M.; Yamaguchi, F. S. M.; Samoto, V. Y.; Han, S. W.; Silva, E. A. Injectable alginate hydrogel for enhanced spatiotemporal control of lentivector delivery in murine skeletal muscle. *J. Controlled Release* **2016**, *237*, 42−49.

(10) Liu, Y.-Y.; Yu, H.-C.; Liu, Y.; Liang, G.; Zhang, T.; Hu, Q.-X. Dual drug spatiotemporal release from functional gradient scaffolds prepared using 3D bioprinting and electrospinning. *Polym. Eng. Sci.* **2016**, *56*, 170−177.

(11) Tibbitt, M. W.; Anseth, K. S. Hydrogels as extracellular matrix mimics for 3D cell culture. *Biotechnol. Bioeng.* **2009**, *103*, 655−663.

(12) Kimna, C.; Lieleg, O. Engineering an orchestrated release avalanche from hydrogels using DNA-nanotechnology. *J. Controlled Release* **2019**, *304*, 19−28.

(13) Scalise, D.; Rubanov, M.; Miller, K.; Potters, L.; Noble, M.; Schulman, R. Programming the Sequential Release of DNA. *ACS Synth. Biol.* **2020**, *9*, 749−755.

(14) Zhang, Z.; Du, J.; Li, Y.; Wu, J.; Yu, F.; Chen, Y. An aptamer-patterned hydrogel for the controlled capture and release of proteins via biorthogonal click chemistry and DNA hybridization. *J. Mater. Chem. B* **2017**, *5*, 5974−5982.

(15) Zhang, Z.; Liu, C.; Yang, C.; Wu, Y.; Yu, F.; Chen, Y.; Du, J. Aptamer-Patterned Hydrogel Films for Spatiotemporally Programmable Capture and Release of Multiple Proteins. *ACS Applied Materials & Interfaces.* **2018**, *10*, 8546−8554.

(16) Dorsey, P. J.; Rubanov, M.; Wang, W.; Schulman, R. Digital Maskless Photolithographic Patterning of DNA-Functionalized Poly-(ethylene glycol) Diacrylate Hydrogels with Visible Light Enabling Photodirected Release of Oligonucleotides. *ACS Macro Lett.* **2019**, *8*, 1133−1140.

(17) Priya James, H.; John, R.; Alex, A.; Anoop, K. R. Smart polymers for the controlled delivery of drugs − a concise overview. *Acta Pharmaceutica Sinica B* **2014**, *4*, 120−127.

(18) Ruiz-Hernández, E.; Baeza, A.; Vallet-Regí, M. Smart Drug Delivery through DNA/Magnetic Nanoparticle Gates. *ACS Nano* **2011**, *5*, 1259−1266.
(19) Murphy, E. B.; Wudl, F. The world of smart healable materials. *Prog. Polym. Sci.* **2010**, *35*, 223−251.
(20) Amaral, A. J. R.; Pasparakis, G. Stimuli responsive self-healing polymers: gels, elastomers and membranes. *Polym. Chem.* **2017**, *8*, 6464−6484.
(21) Uzumcu, A. T.; Guney, O.; Okay, O. Highly Stretchable DNA/Clay Hydrogels with Self-Healing Ability. *ACS Appl. Mater. Interfaces.* **2018**, *10*, 8296−8306.
(22) Schneider, H.-J. Logic-Gate Functions in Chemomechanical Materials. *ChemPhysChem.* **2017**, *18*, 2306−2313.
(23) Yuan, P.; McCracken, J. M.; Gross, D. E.; Braun, P. V.; Moore, J. S.; Nuzzo, R. G. A programmable soft chemo-mechanical actuator exploiting a catalyzed photochemical water-oxidation reaction. *Soft Matter.* **2017**, *13*, 7312−7317.
(24) Paxton, W. F.; Sundararajan, S.; Mallouk, T. E.; Sen, A. Chemical Locomotion. *Angewandte Chemie International Edition.* **2006**, *45*, 5420−5429.
(25) Zarzar, L. D.; Aizenberg, J. Stimuli-Responsive Chemo-mechanical Actuation: A Hybrid Materials Approach. *Acc. Chem. Res.* **2014**, *47*, 530−539.
(26) Cangialosi, A.; Yoon, C.; Liu, J.; Huang, Q.; Guo, J.; Nguyen, T. D.; Gracias, D. H.; Schulman, R. DNA sequence−directed shape change of photopatterned hydrogels via high-degree swelling. *Science.* **2017**, *357*, 1126−1130.
(27) Na, J.-H.; Evans, A. A.; Bae, J.; Chiappelli, M. C.; Santangelo, C. D.; Lang, R. J.; Hull, T. C.; Hayward, R. C. Programming Reversibly Self-Folding Origami with Micropatterned Photo-Crosslinkable Polymer Trilayers. *Adv. Mater.* **2015**, *27*, 79−85.
(28) Yuan, P.; Mao, X.; Chong, K. C.; Fu, J.; Pan, S.; Wu, S.; Yu, C.; Yao, S. Q. Simultaneous Imaging of Endogenous Survivin mRNA and On-Demand Drug Release in Live Cells by Using a Mesoporous Silica Nanoquencher. *Small.* **2017**, *13*, 1700569.
(29) Hsu, B. B.; Jamieson, K. S.; Hagerman, S. R.; Holler, E.; Ljubimova, J. Y.; Hammond, P. T. Ordered and Kinetically Discrete Sequential Protein Release from Biodegradable Thin Films. *Angewandte Chemie International Edition.* **2014**, *53*, 8093−8098.
(30) Lai, J.; Jiang, P.; Gaddes, E. R.; Zhao, N.; Abune, L.; Wang, Y. Aptamer-Functionalized Hydrogel for Self-Programmed Protein Release via Sequential Photoreaction and Hybridization. *Chem. Mater.* **2017**, *29*, 5850−5857.
(31) Wang, H.; Liu, R.; Wang, S.; Guan, Y.; Zhang, Y. A highly programmable platform for sequential release of protein therapeutics. *J. Mater. Chem. B* **2021**, *9*, 1616−1624.
(32) Zhang, D. Y.; Winfree, E. Control of DNA Strand Displacement Kinetics Using Toehold Exchange. *J. Am. Chem. Soc.* **2009**, *131*, 17303−17314.
(33) Zenk, J.; Scalise, D.; Wang, K.; Dorsey, P.; Fern, J.; Cruz, A.; Schulman, R. Stable DNA-based reaction−diffusion patterns. *RSC Advances.* **2017**, *7*, 18032−18040.
(34) Allen, P. B.; Chen, X.; Ellington, A. D. Spatial Control of DNA Reaction Networks by DNA Sequence. *Molecules.* **2012**, *17*, 13390−13402.
(35) Mazzarotta, A.; Caputo, T. M.; Raiola, L.; Battista, E.; Netti, P. A.; Causa, F. Small Oligonucleotides Detection in Three-Dimensional Polymer Network of DNA-PEG Hydrogels. *Gels.* **2021**, *7*, 90.
(36) Hammer, J. A.; Ruta, A.; West, J. L. Using Tools from Optogenetics to Create Light-Responsive Biomaterials: LOVTRAP-PEG Hydrogels for Dynamic Peptide Immobilization. *Ann. Biomed Eng.* **2020**, *48*, 1885−1894.
(37) Liu, J.; Gao, D.; Li, H.-F.; Lin, J.-M. Controlled photo-polymerization of hydrogel microstructures inside microchannels for bioassays. *Lab on a Chip.* **2009**, *9*, 1301−5.
(38) Schaffter, S. W.; Schulman, R. Building in vitro transcriptional regulatory networks by successively integrating multiple functional circuit modules. *Nat. Chem.* **2019**, *11*, 829−838.
(39) Schaffter, S.W.; Chen, K.-L.; O'Brien, J.; Noble, M.; Murugan, A.; Schulman, R. Standardized excitable elements for scalable engineering of far-from-equilibrium chemical networks. *Nat. Chem.* **2022**. DOI: 10.1038/s41557-022-01001-3
(40) Peter, I. S.; Davidson, E. H. Assessing regulatory information in developmental gene regulatory networks. *Proc. Natl. Acad. Sci. U. S. A.* **2017**, *114*, 5862−5869.
(41) Kim, J.; Khetarpal, I.; Sen, S.; Murray, R. M. Synthetic circuit for exact adaptation and fold-change detection. *Nucleic Acids Res.* **2014**, *42*, 6078−6089.
(42) Fern, J.; Schulman, R. Modular DNA strand-displacement controllers for directing material expansion. *Nat. Commun.* **2018**, *9*, 3766.
(43) Lai, S. N.; Zhou, X.; Ouyang, X.; Zhou, H.; Liang, Y.; Xia, J.; Zheng, B. Artificial Cells Capable of Long-Lived Protein Synthesis by Using Aptamer Grafted Polymer Hydrogel. *ACS Synth. Biol.* **2020**, *9*, 76−83.
(44) Xu, Y.; Wang, H.; Luan, C.; Liu, Y.; Chen, B.; Zhao, Y. Aptamer-based hydrogel barcodes for the capture and detection of multiple types of pathogenic bacteria. *Biosensors and Bioelectronics.* **2018**, *100*, 404−410.
(45) Grim, J. C.; Brown, T. E.; Aguado, B. A.; Chapnick, D. A.; Viert, A. L.; Liu, X.; Anseth, K. S. A Reversible and Repeatable Thiol−Ene Bioconjugation for Dynamic Patterning of Signaling Proteins in Hydrogels. *ACS Cent. Sci.* **2018**, *4*, 909−916.
(46) Rosales, A. M.; Anseth, K. S. The design of reversible hydrogels to capture extracellular matrix dynamics. *Nature Reviews Materials.* **2016**, *1*, 15012.
(47) Khademhosseini, A.; Langer, R. A decade of progress in tissue engineering. *Nature Protocols.* **2016**, *11*, 1775−1781.
(48) Monge, C.; Almodóvar, J.; Boudou, T.; Picart, C. Spatio-Temporal Control of LbL Films for Biomedical Applications: From 2D to 3D. *Advanced Healthcare Materials.* **2015**, *4*, 811−830.

https://doi.org/10.1021/acsmaterialslett.2c00286
ACS Materials Lett. 2022, 4, 1807−1814